

Structural, magnetic, and transport investigations of CrTe clustering effect in (Zn,Cr)Te system

M. G. Sreenivasan, K. L. Teo,^{a)} X. Z. Cheng, M. B. A. Jalil, T. Liew, and T. C. Chong
*Information Storage Materials Laboratory, Electrical and Computer Engineering Department,
 National University of Singapore, 4 Engineering Drive 3, Singapore 117576, Singapore
 and Data Storage Institute, 5 Engineering Drive 1, Singapore 117608, Singapore*

A. Y. Du
Institute of Microelectronics, Science Park II, Singapore 117685, Singapore

T. K. Chan and T. Osipowicz
*Physics Department, Faculty of Science, National University of Singapore, CIBA, Block S12,
 2 Science Drive 3, Singapore 117542, Singapore*

(Received 20 March 2007; accepted 13 July 2007; published online 4 September 2007)

We investigate the structural, transport, and magnetic behaviors of (Zn,Cr)Te system without additional carrier doping grown by low temperature molecular-beam epitaxy on GaAs (100) substrates. For the growth of $\text{Zn}_{1-x}\text{Cr}_x\text{Te}$ with $x=0.14$, high-resolution transmission electron microscopy shows the possibility of zinc-blende (ZB)-CrTe phase being embedded in the $\text{Zn}_{1-x}\text{Cr}_x\text{Te}$ matrix. Our detailed analysis of the magnetization results in $\text{Zn}_{0.86}\text{Cr}_{0.14}\text{Te}$ using scaling theory and modified Arrott plots suggests that the ferromagnetic ordering cannot be described by mean-field theory. Additionally, the resistivity behavior indicates that ZB-CrTe clusters could possibly provide a percolative conduction path that gives rise to high Curie temperature. We discussed the ferromagnetism in (Zn,Cr)Te system on the basis of clustering effect. © 2007 American Institute of Physics. [DOI: 10.1063/1.2775535]

I. INTRODUCTION

Tremendous efforts have been made in recent years in the development of diluted magnetic semiconductors (DMSs) as promising candidates for functional semiconductor spintronic devices.^{1,2} One of the major challenges is to obtain a DMS with Curie temperature T_C exceeding the room temperature. Spectacularly, this has led to many reports on high T_C in wide gap DMSs (Ref. 3) in which the nature of ferromagnetism still remains controversial and a consistent picture is thus desired. One of the most common and difficult problems is the identification of magnetisms of different origins and thus the mechanism for ferromagnetism is still intensively investigated.⁴⁻⁸ Additionally, the magnetic percolation in view of disordering effect⁹⁻¹¹ also plays an important role in determining the magnetic as well as transport properties of the DMS systems. In particular, this percolation effect is significant in wide band gap DMSs, where magnetic exchange interactions are short range.

Recent theoretical calculation based on spinodal decomposition^{12,13} has been put forward to explain the high T_C in wide gap DMSs. It has been found that DMS systems are in general unstable against phase separation, therefore the spinodal decomposition phase inherently occurs in DMSs due to strong attractive interactions between impurities. As such in the decomposed phase, a magnetic network can be achieved and high- T_C values can occur in such phases.¹⁴ Experimentally, coherent zinc-blende (ZB)-type MnAs nanoclusters embedded in (Mn,Ga)As matrix have been observed

by transmission electron microscopy (TEM) which leads to high Curie temperature,^{4,5} and the preservation of the hexagonal symmetry in Mn-rich clusters embedded in (Mn,Ga)N has also been reported.⁶ Furthermore, photoemission spectroscopic study has shown that $\text{Ge}_{0.94}\text{Mn}_{0.06}$ is chemically phase separated into the Mn-rich and Mn-depleted phases.⁷ More recently, high Curie ferromagnetism has been reported in self-organized $\text{Ge}_{1-x}\text{Mn}_x$ nanocolumns due to the Ge-rich phase as a result of Mn segregation in the germanium matrix.⁸ All these results point towards the evidence that ferromagnetism (FM) observed in a number of DMS systems may arise from coherent nanoclusters with a large concentration of the magnetic constituent accounting for high apparent Curie temperatures.

In this paper, we report the magnetic and transport measurements as well as detailed TEM investigations on (Zn,Cr)Te system. This material system is of great interest since room-temperature ferromagnetism was reported in $\text{Zn}_{1-x}\text{Cr}_x\text{Te}$,¹⁵ and more recent experiment shows that its FM ordering can be suppressed by nitrogen doping.¹⁶ On the other hand, the effect of iodine doping which is of n type showing a drastic enhancement of the ferromagnetism in $\text{Zn}_{0.95}\text{Cr}_{0.05}\text{Te}$ was reported and its mechanism was discussed on the basis of the double-exchange interaction.¹⁷ Due to the growth of DMSs at relatively low temperatures, there is a high concentration of crystal defects present inevitably in all DMS systems. This causes fluctuations in the carrier densities, particularly in insulating DMSs such as $\text{Zn}_{1-x}\text{Cr}_x\text{Te}$, and hence inhomogeneous magnetic interactions can occur across the material. The recent theoretical prediction shows that the calculated effective chemical pair interactions be-

^{a)}Electronic email: eleteokl@nus.edu.sg

tween Cr impurities in the (Zn,Cr)Te system as a function of distance are attractive and short range, suggesting a tendency toward the phase separation.¹³ We seek to understand the clustering effects that might help achieve magnetic percolation in $\text{Zn}_{1-x}\text{Cr}_x\text{Te}$ that leads to its high T_C . Our results will serve as a direct phenomenological comparison with other DMS systems.

II. EXPERIMENTAL DETAILS

The $\text{Zn}_{1-x}\text{Cr}_x\text{Te}$ films were deposited on semi-insulating GaAs(100) substrates by molecular-beam epitaxy equipped with *in situ* a reflection high energy electron diffraction (RHEED) system to monitor the surface reconstruction during growth. An EPI valved cracking effusion cell is used for elemental tellurium (Te) source, with bulk zone and cracking temperatures operating at 380 and 650 °C, respectively. Zinc (Zn) and chromium (Cr) sources are supplied by low and high temperature effusion cells, respectively. Prior to the growth of $\text{Zn}_{0.86}\text{Cr}_{0.14}\text{Te}$, a 150 nm thick ZnTe is used as a buffer. The substrate temperature during growth was 150–200 °C and the growth rate is ~ 12 nm/min. The thickness of the $\text{Zn}_{0.86}\text{Cr}_{0.14}\text{Te}$ thin film is ~ 0.75 μm . No intentional doping was used throughout the present work. Another batch of CrTe films of 100 nm thickness was also grown on GaAs (100) substrates via ZnTe buffer layer at 150–200 °C. The structural properties of the films were investigated using high-resolution transmission electron microscopy (HRTEM) and selected-area electron diffraction (SAED). Magnetization measurements as a function of temperature were performed using a commercial superconducting quantum interference device (SQUID) magnetometer. In order to determine the diamagnetic component of the magnetization signals from the samples, the susceptibility of a bare GaAs substrate that was used for the growth was measured. The obtained value of susceptibility $\chi = -2.77 \times 10^{-6}$ cm^3/g is subsequently used in the subtraction of the diamagnetic background for all the samples. The resistivity (ρ) was measured by the usual four probe method. The Cr concentration of the films was determined by particle induced x-ray emission (PIXE) measurement.

III. RESULTS AND DISCUSSIONS

Figure 1 shows the PIXE spectrum of a standard sample obtained with a 2 MeV proton beam from the HVEE 3.5 MV singletron accelerator at NUS.¹⁸ The sample was tilted 20° with respect to the incident beam and the emitted x rays were collected with a 65 mm^2 Si(Li) detector at 135°. A 50 mm Kapton foil is used to filter out low energy x rays, and a passivated implanted planar silicon (PIPS) detector placed at 20° measured a Rutherford backscattering spectroscopy (RBS) spectrum simultaneously that was used for charge normalization. A clear Cr peak is observed, and a subsequent fit of the spectrum with the GUPIX quantification code¹⁹ reveals a Cr concentration of 14% of the top layer. Other samples with different Cr concentrations used in our studies are similarly obtained by this method.

Figure 2(a) shows the cross-sectional TEM image of the CrTe films. In this picture, the highly oriented crystalline

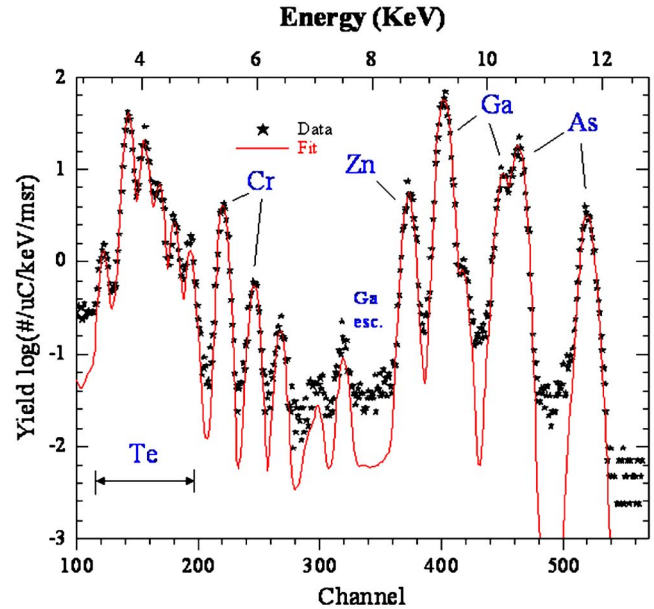


FIG. 1. (Color online) PIXE Result and element fitting for sample with Cr doping concentration of 0.14.

CrTe grains are embedded in the amorphous matrix. These grains are oriented at an angle of 55° to the surface of GaAs (100) which is the exact (111) plane of GaAs and the (111)ZnTe buffer layer. This clearly shows that the ZnTe {111} plane is used as the seed of the CrTe grains. The nucleation of CrTe is thus suspended due to the low growth temperature. Figure 2(b) shows the image at some restricted areas of the interface. The results clearly indicate that the coherent lattice matching between the ZnTe and CrTe layers is preferentially oriented in the $\langle 111 \rangle$ directions. Figure 2(c) shows the SAED patterns of the CrTe and ZnTe buffer lay-

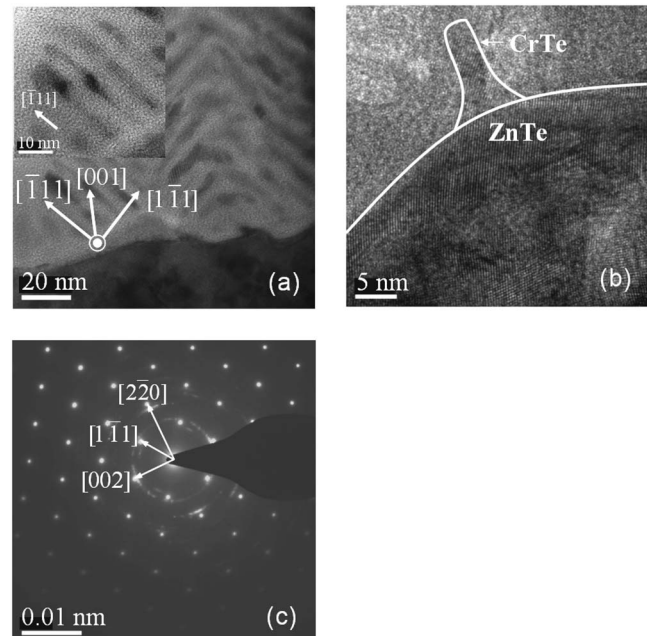


FIG. 2. (a) Cross-sectional TEM image of the CrTe/ZnTe. The inset shows the magnified image of the CrTe layer. (b) TEM image near the CrTe and ZnTe interface. (c) SAED pattern for the CrTe film.

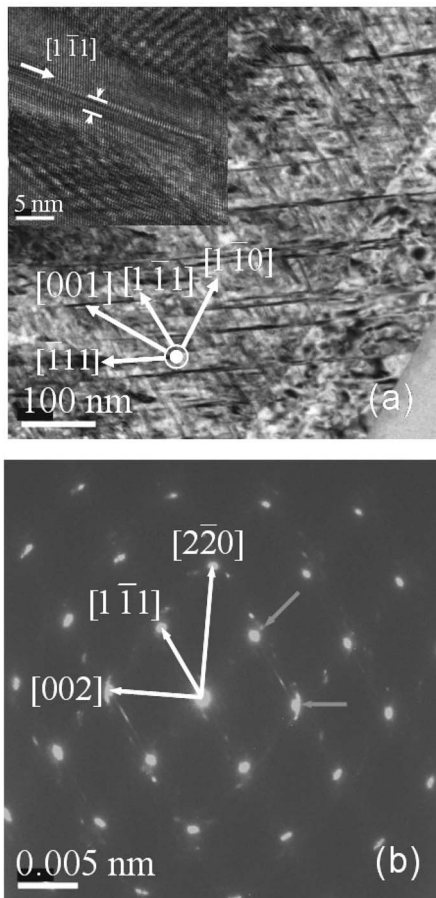


FIG. 3. (a) Cross-sectional TEM image of $\text{Zn}_{0.84}\text{Cr}_{0.14}\text{Te}$. The inset shows the magnified image of the defect region. (b) SAED pattern for the $\text{Zn}_{0.86}\text{Cr}_{0.14}\text{Te}$ film.

ers. In addition to the main diffraction spots due to the zincblende (ZB)-ZnTe buffer layer, the partial rings that are present along certain directions indicate the presence of another set of reflections that is due to the ZB-CrTe phase. Our results suggest that CrTe, which has NiAs related structures in its bulk phase, has formed a coherent ZB structure with preferred orientation in the $\langle 111 \rangle$ direction of the ZnTe buffer layer.

Figures 3(a) and 3(b) show the cross-sectional TEM image and the SAED pattern of the $\text{Zn}_{0.86}\text{Cr}_{0.14}\text{Te}$ layer. We observe a very high density of precipitations along the ZnTe $\{111\}$ plane in the $\text{Zn}_{0.86}\text{Cr}_{0.14}\text{Te}$ layer, as shown in Fig. 3(a). Additionally, stacking faults are observed in the ZnTe buffer layer which propagates into the ZnCrTe layer, but its density is very low as compared with those of the precipitated regions. The inset of Fig. 3(a) shows the magnified image of the precipitated region in the $\text{Zn}_{0.86}\text{Cr}_{0.14}\text{Te}$ layer. The thickness of this region is approximately 20 \AA , which is much less than the critical thickness required for the relaxation of the lattice. The moiré patterns are also observed in the surrounding regions due to the high density of the precipitation in the $\{111\}$ plane. Figure 3(b) exhibits the regular diffraction spots of ZB $\text{Zn}_{0.86}\text{Cr}_{0.14}\text{Te}$ together with an additional phase (marked by gray arrows) originating from the coherent ZB-CrTe structure. The precipitated regions containing the coherent ZB-CrTe clusters in the ZnCrTe layer form as precipi-

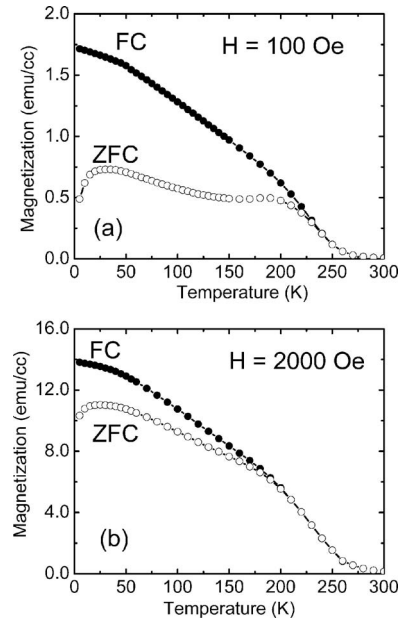


FIG. 4. Zero-field-cooled (ZFC) and field-cooled (FC) magnetization curves for $\text{Zn}_{0.86}\text{Cr}_{0.14}\text{Te}$ film at (a) 100 Oe and (b) 2000 Oe.

tates along the ZB-ZnTe $\{111\}$ plane, which is in good correlation with that of the as-grown CrTe layer. Based on the d spacing of the SAED patterns in Figs. 2(c) and 3(b), we obtained the lattice constants of ZB $\text{Zn}_{0.86}\text{Cr}_{0.14}\text{Te}$ and ZB CrTe to be 6.17 and 6.65 Å , respectively.

Figures 4(a) and 4(b) present the zero-field-cooling (ZFC) and field-cooling (FC) curves of $\text{Zn}_{0.86}\text{Cr}_{0.14}\text{Te}$ thin film at two different applied fields. The deviation of the ZFC and FC curves at a lower magnetic field (100 Oe) demonstrates superparamagnetic behavior. It is likely that there exist FM precipitates inside the film. In addition, the shapes of the FC curves deviate from the Weiss mean-field theory, which strongly indicates the effect of localization in the presence of disorder.⁹ This suggests that the exchange interactions inside the samples may not be homogeneous. We attempt to fit the $1/\chi-T$ curve to the Curie-Weiss law and the intercept on the temperature axis at the positive side gives $\theta_p = 265 \text{ K}$.

Figure 5 shows the $M-T$ curve of the CrTe film at an applied field of 100 Oe and the inset shows the $M-H$ loop at 5 K. From the dependence of M^2 versus temperature, the Curie temperature T_C^* for the as-grown CrTe films is found to

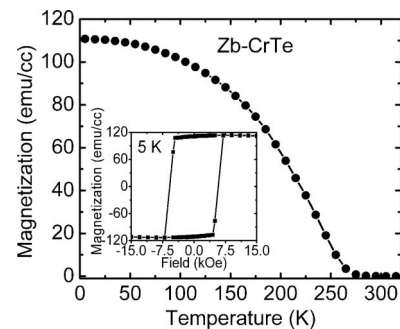


FIG. 5. The $M-T$ curve of CrTe film at 100 Oe. The inset is the $M-H$ loop at 5 K.

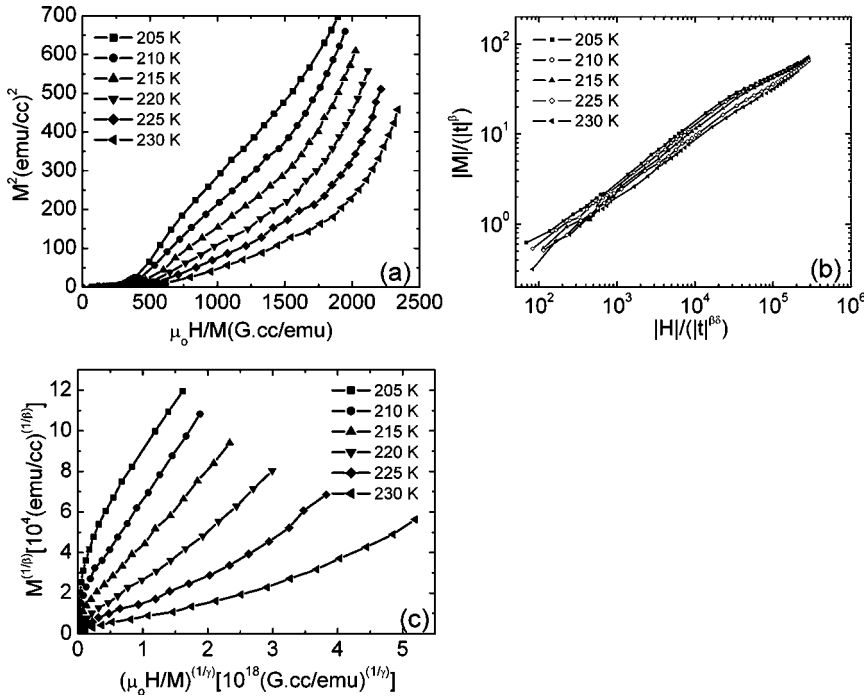


FIG. 6. Conventional Arrott plot for $\text{Zn}_{0.86}\text{Cr}_{0.14}\text{Te}$ sample using the critical components from mean-field approximation ($\beta=0.5$ and $\gamma=1$). (b) Scaling plot of $|M|/|t|^\beta$ vs $|H|/|t|^{\beta\delta}$. (c) Modified Arrott plot constructed using critical exponents $\delta=1.64$, $\beta=0.28$, and $\gamma=0.18$.

be ~ 247 K. It is noteworthy that the T_C^* for bulk $\text{Cr}_{1-\delta}\text{Te}$ in NiAs phases is in the region of 315–360 K.²⁰ There was no indication of the NiAs phase in the high-resolution x-ray diffraction scan of our samples. The presence of NiAs-type CrTe will also usually show a bulk behavior with Curie temperature above 300 K. From the value of the saturation magnetization at 5 K, the saturated moment M_o ($=g\mu_B S$) per Cr atom is estimated to be $0.97\mu_B$ and $0.96\mu_B$ for CrTe and $\text{Zn}_{0.86}\text{Cr}_{0.14}\text{Te}$, respectively. Using a g factor of 2, we can see that the spin $S \sim 1/2$, which is a factor of 4 less than the $S=2$ for the divalent Cr. This can be attributed to the disordering effects leading to the participation of only a small percentage of Cr ions in the ferromagnetism.

Figure 6(a) shows the Arrott plots obtained for the $\text{Zn}_{0.86}\text{Cr}_{0.14}\text{Te}$ films which exhibit considerable curvatures making the identification of T_C ambiguous. Such a trend is usually observed in a disordered system having a broad distribution of exchange coupling strengths.²¹ It is noteworthy that the influence of the diamagnetic contribution from the GaAs substrates to the magnetization signals of $\text{Zn}_{0.86}\text{Cr}_{0.14}\text{Te}$ films is insignificant but nevertheless, it has been subtracted from the measured results. A modified Arrott plot analysis is adopted^{22,23} to establish the ferromagnetic ordering in the film. This is carried out by plotting $M^{1/\beta}$ vs $(H/M)^{1/\gamma}$ where the critical exponents β and γ are based on the Arrott-Noakes equation of state.²⁴ These are related to a third parameter δ by the Widom scaling relation $\delta=1+\gamma/\beta$.²⁵ The δ value has been determined using the relation $M \sim H^{1/\delta}$ ($T=T_C$) and plotting $d \ln(\mu_o H)/d \ln(M)$ vs $\mu_o H$ for the (M, H) data at different temperatures. The isotherm which yields a slope closest to zero corresponds to $T=T_C$ and the average values of $d \ln(\mu_o H)/d \ln(M)$ above $\mu_o H=500$ Oe gives δ . Using this method, the T_C and the δ values are obtained to be 220 ± 7 K and 1.64 ± 0.07 , respectively. As shown in Fig. 6(b), scaling plots have been made in which the (M, H) data are plotted as a function of $|M|/|t|^\beta$

vs $|H|/|t|^{\beta\delta}$ where $t=(T-T_C)/T_C$ and finding the best fit values of β and δ for which all the data points fall on one universal curve with two branches, one corresponding to $T < T_C$ and the other corresponding to $T > T_C$. The parameters thus determined are $\delta=1.64 \pm 0.07$, $\beta=0.28 \pm 0.02$, and $\gamma=0.18 \pm 0.02$ using $T_C=220 \pm 7$ K. Figure 6(c) shows the modified Arrott plot constructed using these critical exponents. This analysis strongly indicates that the ferromagnetic ordering is not described by mean-field critical components of $\beta=0.5$, $\delta=3$, and $\gamma=1$ and also do not agree with those of three-dimensional (3D) Heisenberg model for which $\beta=0.3645$, $\delta=4.8$, and $\gamma=1.386$.²⁶ Although, the β parameter seems to be closer to the 3D Ising model ($\beta=0.325$, $\delta=5$, and $\gamma=1.24$),²⁶ the parameters δ and γ are not in agreement. We suggest that such a deviation from mean-field behavior may be due to the presence of clustering effects or impurity phase arising from phase separation.

We have measured the resistivity (ρ) as a function of temperature and magnetic field for $\text{Zn}_{0.86}\text{Cr}_{0.14}\text{Te}$ and as-grown CrTe films. We note that our $\text{Zn}_{1-x}\text{Cr}_x\text{Te}$ samples for $x=0.026$, 0.035 , and 0.12 are highly resistive, exhibiting nor-

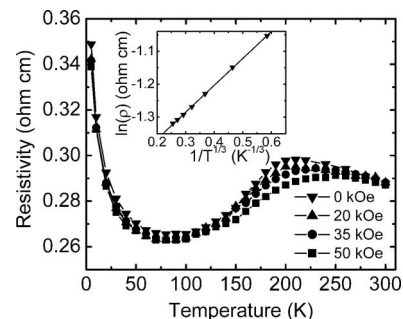


FIG. 7. The resistivity of $\text{Zn}_{0.86}\text{Cr}_{0.14}\text{Te}$ measured with and without magnetic field dependence as a function of temperature. The inset is the plot of $\ln \rho$ vs $T^{-1/3}$.

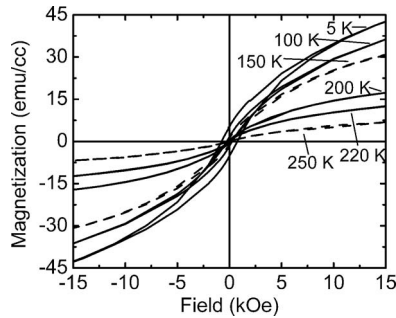


FIG. 8. M - H loops of $\text{Zn}_{0.86}\text{Cr}_{0.14}\text{Te}$ measured at various temperatures.

mal insulating behavior ($\sim 10^3 \Omega \text{ cm}$ at RT), while the ρ values of as-grown CrTe films are metallic ($\sim 10^{-3} \Omega \text{ cm}$ at RT). Previous reports have shown that $\text{Zn}_{1-x}\text{Cr}_x\text{Te}$ without additional carrier doping is insulating²⁷ and the resistivity is several orders of magnitudes higher than those of $\text{In}_{1-x}\text{Mn}_x\text{As}$ (Ref. 28) and $\text{Ga}_{1-x}\text{Mn}_x\text{As}$.²⁹ As such, its origin cannot be attributed to the carrier-induced mechanism, different from the case of Mn-doped III-V semiconductors,³⁰ but rather a double-exchange mechanism has been invoked to explain the FM behavior in the $\text{Zn}_{1-x}\text{Cr}_x\text{Te}$ system.¹⁶ Figure 7 shows the ρ vs T plot with and without magnetic field for $\text{Zn}_{0.86}\text{Cr}_{0.14}\text{Te}$. Besides the insulating trend at lower temperatures, the ρ is accompanied by a broad maximum at around $T_C \sim 220$ K. This feature has been commonly observed in group III-V and IV magnetic semiconductors^{31,32} around the ferromagnetic Curie temperature T_C and has been attributed to spin-related scattering. The T_C value obtained agrees well with the corresponding value obtained from the Arrott plot. Our resistivity behavior appears to be dirty metalliclike, which is likely due to the weak localization effect of disordering. We have fitted the low temperature range (5–60 K) using the function $\ln \rho = \rho_0 \exp(\alpha T^{1/n})$, with $n=2$, 3 or 4.³³ The corresponding value of $n=3$ gives the best least-squares fit, as shown in the inset of Fig. 7. This is the characteristic of transport occurring by phonon-assisted carrier hopping between localized states.

We have measured the M - H loops at different temperatures and found that FM ordering indeed ceases to exist at $T_C \sim 220$ K, as shown in Fig. 8. Taking into account TEM images results and disordering effect observed in our Arrott plots, we suggest that the resistivity behavior could be due to percolative conduction through the presence of ZB-CrTe clusters region within the $\text{Zn}_{0.86}\text{Cr}_{0.14}\text{Te}$ matrix. Additionally, the paramagnetic Curie temperature θ_p ($=265$ K) is higher than the ferromagnetic T_C ($=220$ K) which indicates that magnetic short-range order remains even above T_C . The origin of short-range ordering possibly comes from the precipitation of FM CrTe clusters.

IV. CONCLUSIONS

In summary, we have studied the structural, magnetic and transport properties of the (Zn,Cr)Te system. The resistivity behavior, high-resolution TEM images, and modified

Arrott plot analyses suggest that the FM ordering in $\text{Zn}_{0.86}\text{Cr}_{0.14}\text{Te}$ could arise from CrTe clustering in our samples. We propose that the magnetic network in $\text{Zn}_{0.86}\text{Cr}_{0.14}\text{Te}$ could possibly be achieved via ferromagnetic CrTe clusters. Our results highlight the importance of clustering effect in models for the DMS system and hence potential considerable influence of disorder on the Curie temperature.

ACKNOWLEDGMENT

This work is supported by the Singapore Agency for Science, Technology and Research (A*STAR) under Grant No. 052-101-0100.

- ¹S. A. Wolf, D. D. Awschalom, R. A. Buhrman, J. M. Daughton, S. von Molnar, M. L. Roukes, A. Y. Chtchelkanova, and D. M. Treger, *Science* **294**, 1488 (2001).
- ²T. Dietl, H. Ohno, F. Matsukura, J. Cibert, and D. Ferrand, *Science* **287**, 1019 (2000).
- ³S. J. Pearton *et al.*, *J. Appl. Phys.* **93**, 1 (2003).
- ⁴M. Moreno, A. Trampert, B. Jenichen, L. Daweritz, and K. H. Ploog, *J. Appl. Phys.* **92**, 4672 (2002).
- ⁵M. Yokoyama, H. Yamaguchi, T. Ogawa, and M. Tanaka, *J. Appl. Phys.* **97**, 10D317 (2005).
- ⁶G. Martinez-Criado *et al.*, *Appl. Phys. Lett.* **86**, 131927 (2005).
- ⁷J.-S. Kang *et al.*, *Phys. Rev. Lett.* **94**, 147202 (2005).
- ⁸M. Jamet *et al.*, *Nat. Mater.* **5**, 653 (2006).
- ⁹S. Das Sarma, E. H. Hwang, and A. Kaminski, *Phys. Rev. B* **67**, 155201 (2003).
- ¹⁰A. Kaminski and S. Das Sarma, *Phys. Rev. B* **68**, 235210 (2003).
- ¹¹L. Bergqvist, O. Eriksson, J. Kudrnovský, V. Drchal, P. Korzhavyi, and I. Turek, *Phys. Rev. Lett.* **93**, 137202 (2004).
- ¹²K. Sato, H. Katayama-Yoshida, and P. H. Dederichs, *Jpn. J. Appl. Phys., Part 2* **44**, L948 (2005).
- ¹³T. Fukushima, K. Sato, H. Katayama-Yoshida, and P. H. Dederichs, *Jpn. J. Appl. Phys., Part 2* **45**, L416 (2006).
- ¹⁴T. Dietl, *Nat. Mater.* **5**, 673 (2006).
- ¹⁵H. Saito, V. Zayets, S. Yamagata, and K. Ando, *Phys. Rev. Lett.* **90**, 207202 (2003).
- ¹⁶N. Ozaki, I. Okabayashi, T. Kumekawa, N. Nishizawa, S. Marcet, S. Kuroda, and K. Takita, *Appl. Phys. Lett.* **87**, 192116 (2005).
- ¹⁷N. Ozaki, N. Nishizawa, S. Marcet, S. Kuroda, O. Eryu, and K. Takita, *Phys. Rev. Lett.* **97**, 037201 (2006).
- ¹⁸F. Watt, J. A. van Kan, I. Rajta, A. A. Bettiol, T. F. Choo, M. B. H. Breese, and T. Osipowicz, *Nucl. Instrum. Methods Phys. Res. B* **210**, 14 (2003).
- ¹⁹J. A. Maxwell, W. J. Teesdale, and J. L. Campbell, *Nucl. Instrum. Methods Phys. Res. B* **95**, 407 (1995).
- ²⁰J. Dijkstra, H. H. Weitering, C. F. van Brugger, C. Haas, and R. A. de Groot, *J. Phys.: Condens. Matter* **1**, 9141 (1989).
- ²¹I. Yeung, R. M. Roshko, and G. Williams, *Phys. Rev. B* **34**, 3456 (1986).
- ²²V. Tsurkan, M. Baran, A. Szewczyk, R. Szymczak, and H. Szymczak, *J. Phys.: Condens. Matter* **11**, 7907 (1999).
- ²³W. M. Yuhasz *et al.*, *Phys. Rev. B* **71**, 104402 (2005).
- ²⁴A. Arrott and J. E. Noakes, *Phys. Rev. Lett.* **19**, 786 (1967).
- ²⁵B. Widom, *J. Chem. Phys.* **43**, 3892 (1965).
- ²⁶J. C. Le Guillou and J. Zinn-Justin, *Phys. Rev. B* **21**, 3976 (1980).
- ²⁷H. Saito, S. Yamataga, and K. Ando, *J. Appl. Phys.* **95**, 7175 (2004).
- ²⁸H. Ohno, H. Munekata, T. Penney, S. von Molnar, and L. L. Chang, *Phys. Rev. Lett.* **68**, 2664 (1992).
- ²⁹A. Oiwa *et al.*, *Solid State Commun.* **103**, 209 (1997).
- ³⁰T. Dietl, *Semicond. Sci. Technol.* **17**, 377 (2002).
- ³¹F. Matsukura, H. Ohno, A. Shen, and Y. Sugawara, *Phys. Rev. B* **57**, R2037 (1998).
- ³²A. P. Li, J. Shen, J. R. Thompson, and H. H. Weitering, *Appl. Phys. Lett.* **86**, 152507 (2005).
- ³³T. G. Castner, in *Hopping Transport in Solids*, edited by M. Pollak and B. I. Shklovskii (Elsevier, New York/North-Holland, Amsterdam, 1990), p. 1.